NANO LETTERS

2005 Vol. 5, No. 5 957–961

Surface Plasmon Interference Nanolithography

Zhao-Wei Liu,† Qi-Huo Wei,‡ and Xiang Zhang*,†

NSF Nanoscale Science and Engineering Center (NSEC), 5130 Etcheverry Hall, University of California, Berkeley, California 94720-1740, and Applied NanoBioscience Center, Arizona State University, Main Campus, P.O. Box 874004, Tempe, Arizona 85287-4004

Received March 31, 2005; Revised Manuscript Received April 7, 2005

ABSTRACT

A new nanophotolithography technique based on the interference of surface plasmon waves is proposed and demonstrated by using computer simulations. The wavelengths of the surface plasmon waves at metal and dielectric interfaces can reach the nanometer scale while their frequencies remain in the optical range. As a result, the resolution of this surface plasmon interference nanolithography (SPIN) can go far beyond the free-space diffraction limit of the light. Simulation results show that one-dimensional and two-dimensional periodical structures of 40–100 nm features can be patterned using interfering surface plasmons launched by 1D gratings. Detailed characteristics of SPIN such as field distribution and contrast are also investigated.

As the most widely used form of lithography for almost all micromanufacturing purposes, photolithography was limited by the physics of diffraction. To achieve nanometer feature sizes, either the working wavelength has to be reduced, 1-3 or alternative techniques of pattern transfer such as nanoimprinting lithography (NIL)4,5 have to be adopted. The main approach to reducing the working wavelength is to directly use light sources of higher photon energy such as extreme ultraviolet light (EUV) or soft X-rays. 1-3,6-7 However, accompanying with this reduction of the exposing wavelengths is the drastic increase of complexity and cost for instrumentation and processing. Another approach, called immersion photolithography, 1-3,8-9 interposes a liquid medium between the optics and the wafer surface to replace the usual air gap. Even though the wavelength of the light can be reduced by a factor equal to the refractive index of the liquid, the resolution improvement is limited owing to the relative low refractive index of the available materials. It has also been shown that a solidimmersion lens could be used for increasing the resolution of photolithography.¹⁰

A new scheme to achieve photolithographic nanopatterning is proposed recently,^{11–13} which is based on the unique properties of surface plasmons (SP). The dispersion relation for the surface plasmons at an interface between semi-infinite metal and dielectric materials can be written as:¹⁴

$$k_{\rm sp} = k_0 \sqrt{\frac{\epsilon_{\rm m} \epsilon_{\rm d}}{\epsilon_{\rm m} + \epsilon_{\rm d}}} \tag{1}$$

where $k_{\rm sp}$ and k_0 are the wave vectors of the surface plasmons and the light of the same frequency in a vacuum. $\epsilon_{\rm m}$ and $\epsilon_{\rm d}$ are the permittivities of the metal and dielectric materials, respectively. Owing to the collective excitations of conduction electrons in metals such as Au, Ag, and Al, $\epsilon_{\rm m}$ for these metals is strongly wavelength dependent and negative at optical frequencies. The wave vector of surface plasmons can thus become significantly larger than that of the free space light at the same frequency when the real part of $\epsilon_{\rm m}$ approaches $-\epsilon_{\rm d}$. The frequency at which ${\rm Re}(\epsilon_{\rm m}) = -\epsilon_{\rm d}$ is called the resonant surface plasmon frequency $\omega_{\rm sp}$. At frequencies close to $\omega_{\rm sp}$, surface plasmons possess "an optical frequency, but a down to X-ray wavelength". As a result, utilizing surface plasmon waves for lithography may dramatically increase the pattern resolution.

Lately it was demonstrated that the use of surface plasmons in the optical near field of a metallic mask can produce fine patterns with a subwavelength resolution. ^{12,15,16} Especially, using a silver grating mask with 300 nm periodicity, lithography with 100 nm pitch has been demonstrated by using the interference of surface plasmon waves within the grating area. ¹⁵

In this paper, we numerically demonstrate surface plasmon interference nanolithography (SPIN). In contrast to previous work, 12-13,15-16 multiple one-dimensional gratings are used to convert free-space light into surface plasmon waves, and

^{*} Corresponding author, E-mail: xiang@berkeley.edu

[†] University of California, Berkeley.

[‡] Arizona State University.

those waves propagating outside the grating area form an interference pattern when they encounter each other. By using a different number of gratings or surface plasmon waves, various interference patterns such as periodic lines and two-dimensional dot arrays can be obtained. The numerical results show that the resolution can go far beyond the free-space diffraction limit by tuning the excitation light frequency close to the resonant surface plasmon frequency. This SPIN technique promises various practical fabrication applications since it only requires UV photoresists.

Numerical simulations were performed using the commercial software package CST Microwave Studio (MWS). With the aim of validating the simulation method and reviewing quantitatively some fundamental properties of surface plasmon waves, which are important to SPIN, we first studied a simple situation where only a one-dimensional grating is used.

The simulated structure consists of a transparent glass as the mask substrate, an aluminum mask, and a semi-infinite photoresist (PR) layer (Figure 1a). The thickness of the Al mask is assumed to be 100 nm, which is sufficiently thick to block the direct transmitted light, ensuring that all fields at the Al/PR interfaces outside the gratings originate from surface plasmon waves and that the Al film can be treated as semi-infinite. Ag is another good material candidate for SPIN mask considering its plasmon frequency $\omega_{\rm sp}$ is also located at UV range (Au mask is not appropriate for lithography purposes because its $\omega_{\rm sp}$ locates at visible range). Al is chosen as an example here because of its relatively long SP propagation length at UV excitation. A onedimensional grating with periodicity Λ is used so that the momentum difference between the incident light and the surface plasmons can be compensated.

The refractive indices used for the glass and the PR (from AZ Electronic Materials data sheets for AZ5200-E) are 1.52 and 1.7, respectively. The permittivity of the Almask is described by the Drude model, $\epsilon_{\rm Al}(\omega) = \epsilon_{\infty} - \omega_{\rm p}^2/[\omega(\omega-iV_{\rm c})]$, where the high-frequency bulk permittivity $\epsilon_{\infty}=1$, the bulk plasmon frequency $\omega_{\rm p}=2.4\times10^{16}{\rm rad/s}$, and the electron collision frequency $V_{\rm c}=1.1\times10^{15}{\rm rad/s}$, are obtained by fitting the model to the experimental data taken from the literature. The incident light, polarized along the x direction or perpendicular to the grating, is normal to the substrate. Based on the conservation of momentum, surface plasmon waves with a wave vector $k_{\rm sp}=2\pi/\Lambda$ can be resonantly excited.

The electrical field magnitudes at the Al/PR interface at different distances from the grating edges are shown in Figure 1b as functions of the excitation frequencies. For a grating with the period $\Lambda=205$ nm, clear resonant peaks can be seen around the frequency 8.22×10^{14} Hz, or a vacuum excitation wavelength at 365 nm (Figure 1b,c). From the local field distribution at the frequency 8.22×10^{14} Hz, surface plasmon waves can be observed propagating and decaying in magnitudes with the distance away from the grating edge (Figure 1d).

Key physical parameters obtained from this simulation agree well with analytical predictions. (1) For a grating with

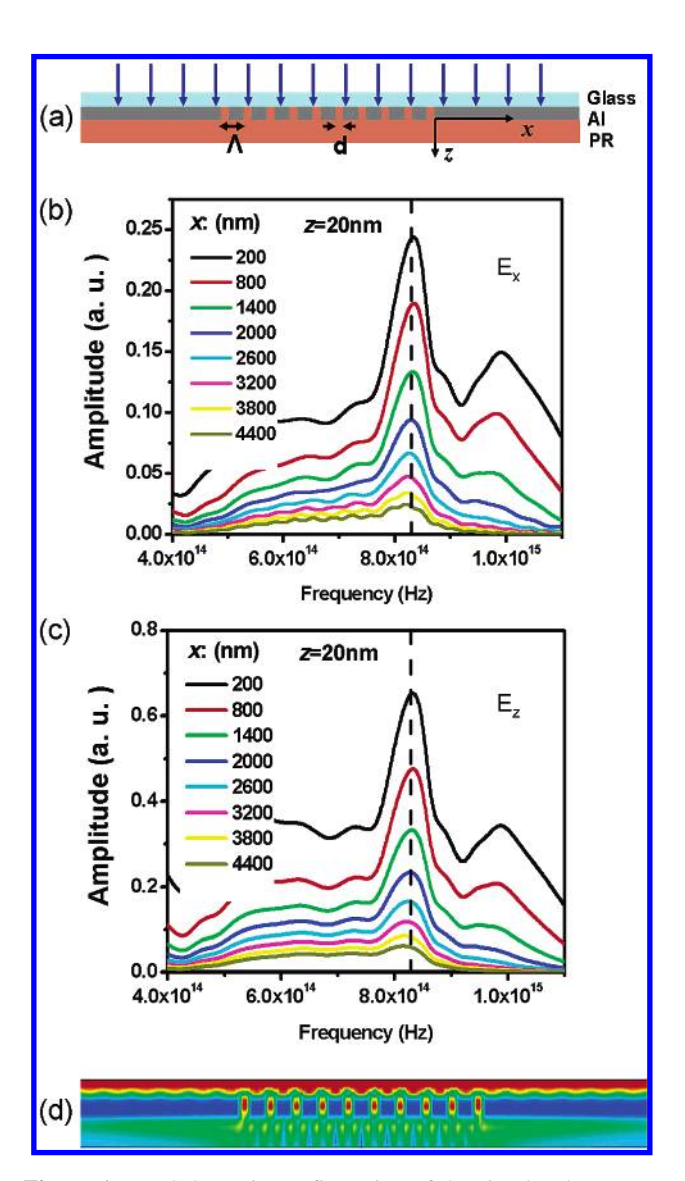


Figure 1. (a) Schematic configuration of the simulated structure which is composed of a transparent glass substrate, a 100 nm thick aluminum mask, and a semi-infinite photoresist. The grating periodicity Λ is 205 nm and the grating slit d is 60 nm. The amplitudes of electric field components (b) E_x and (c) E_z versus the excitation frequency at 20 nm away from the Al/PR interface and at different x positions. (d) Cross-section of the total electric field distribution at the frequency $f = 8.22 \times 10^{14}$ Hz.

period $\Lambda = 205$ nm, theoretical calculations based on eq 1 yield a resonant excitation wavelength at $\lambda = 377$ nm, which agrees with the simulation result within 3%. This slight deviation in the resonant wavelength is ascribed to the coarse meshing size in the simulation. (2) The propagation length along the surface, which dictates the maximum interference area with sufficient contrasts, is obtained by exponential fitting to the electrical field curve versus the distance from the grating (Figure 2a). The simulation results yield about 1.8 μ m propagation length for both E_x and E_z , which agrees with the theoretical prediction $1/\{Im\}(k_{sp}) \sim 1.74 \mu m.$ (3) The decay length of SP waves in the z direction, on the other hand, determines the exposure depth in the photoresist. The simulation data (Figure 2b) yield approximately 84 nm for both E_x and E_z , while the theoretical estimation $1/|k_z|$ $\lambda/2\pi|\sqrt{(\epsilon'_{\rm Al}+\epsilon_{\rm PR})/(\epsilon_{\rm PR}^2)}|$ is about 82.3 nm. (4) The ratio $E_z/2\pi$

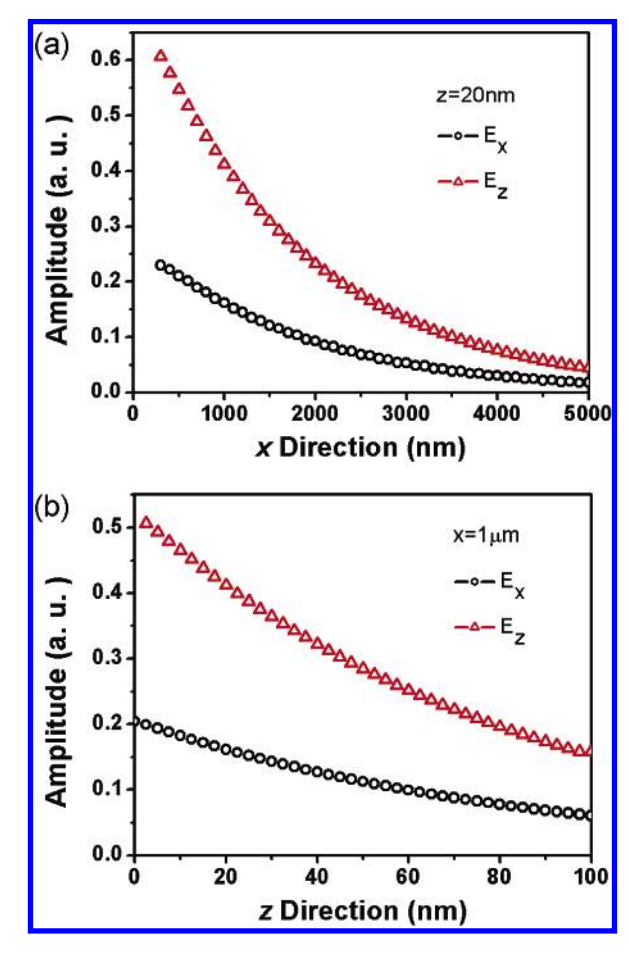


Figure 2. (a) Amplitudes of the electric fields at $f = 8.22 \times 10^{14}$ Hz versus the horizontal distance x from the grating at constant vertical distance z = 20 nm. (b) Amplitude of the electric fields at $f = 8.22 \times 10^{14}$ Hz versus the vertical distance z from the Al/PR interface at constant $x = 1 \mu m$.

 E_x affects the interference contrasts as discussed later and is determined by the permittivities of Al and the photoresist, $E_z/E_x = -k_x/k_z = -i\sqrt{(|\epsilon'_{\rm Al}|)/(\epsilon_{\rm PR})}$. The simulated $E_z/E_x = 2.61$ agrees with the theoretical prediction 2.62. All of these agreements between theoretical calculations and the simulation results suggest the validity of the simulations.

Next, we consider the surface plasmon interference. When two counter propagating surface plasmon waves meet, interference fringes are formed. The periodicity d of the interference fringes are half of the surface plasmon wavelength; i.e., $d = \lambda_{\rm sp}/2 = \lambda_0 k_0/2k_{\rm sp}$. Therefore, in comparison with direct laser interference lithography (LIL), $^{18-20}$ the resolution of SPIN is enhanced by a factor of $k_{\rm sp}/k_0$.

Two parallel gratings are used to excite two counter propagating surface plasmon waves, and the separation between them is $2 \mu m$, which is about the propagation length of the SP waves at the excitation frequency. The electrical field distribution (Figure 3) clearly shows that a standing wave or an interference pattern with a $\sim \! 100$ nm periodicity is formed within 100 nm thick photoresit at the interface. Under the exposure of this spatially modulated electromagnetic field (Figure 3d), parallel lines with approximately sinusoidal profile and 100 nm periodicity can be developed in the photoresist. If the half peak width is taken as the

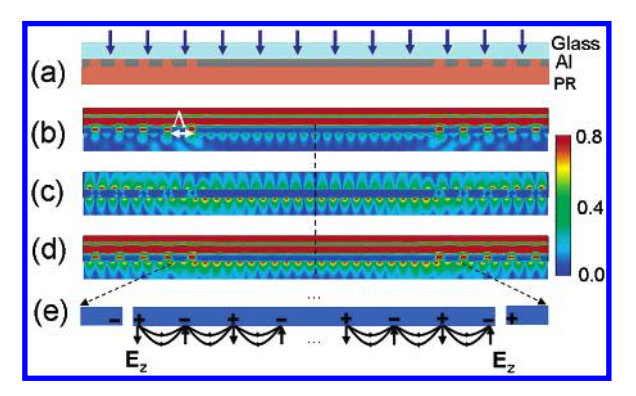


Figure 3. (a) Schematic configuration of the simulated structure which comprises of two parallel gratings with 2 μ m separation. Other parameters are the same as those in Figure 1a. (b), (c), (d) Cross sections of the electrical field amplitude distributions for E_x , and E_z , and E_z , respectively. (e) Schematic drawing of the temporary charge and electrical field distributions of the surface plasmon waves propagating away from the grating slits.

feature size, features about 1/7 of the excitation wavelength can be reached.

It is worth pointing out that interference fringes of E_x and E_z components have a half wavelength shift in space (Figure 3b and c). This originates from the characteristics of the surface plasmon waves as schematically shown in Figure 3e. The charges accumulated at two edges of the grating slits always have opposite signs, meaning the E_z waves emitted from the left and right sides have a 180° phase difference, while the E_x waves are the same in phase. As a result, at the center point between the gratings, the interference standing wave is always at its minimum for E_z components while at its maximum for E_x components.

Since the photoresist is only sensitive to the total optical field intensity (i.e., $|E_z|^2+|E_x|^2$), E_z/E_x must be be high (or low) enough to provide sufficient intensity contrast. Fortunately, with the Al mask and the AZ photoresist used, $|E_z|^2/|E_x|^2$ is about 7; therefore, the total intensity is dominated by the E_z components. The intensity contrast of the interference is larger than 0.7 at the middle while it drops to about 0.5 close to the grating edges. Given the fact that typical minimum contrasts required for common negative optical resists are around 0.2,²¹ the contrast of surface plasma interference is sufficiently high for lithography purposes.

If two gratings are considered as partially reflective mirrors similar to those in a laser cavity, it can be expected that the interference contrast will be affected by the grating separation. To investigate this dependency, we performed simulations with different grating separations L. The results show that the field intensities display a series of resonant levels at certain separations, a phenomenon similar to a laser cavity effect (Figure 4a). This behavior, however, differs from that of a laser cavity in two major aspects. First, the separation difference between two adjacent resonances is equal to SP wavelengths (Figure 4b) in stead of half SP wavelengths as in the laser cavity. This is because the interference pattern here originates from two counter propagating waves from both left and the right gratings. While in the laser cavity, only one original wave is counted for the interference. Second, in contrast to the laser cavity where the peak

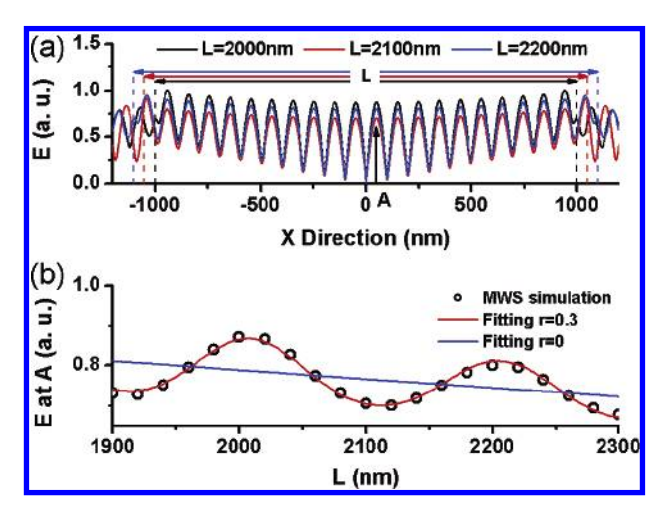


Figure 4. (a) Total electric fields at constant vertical distance from the Al/PR interface (z=20 nm) for three different grating separations L=2000 nm, 2100 nm, and 2200 nm. The vertical dashed lines indicate the locations of the grating edges. (b) The electric field at point A (x=50 nm) versus the grating separation L. Black circles are the simulated results while the red and blue curves are the fitting results using eq 2. The parameters used in this fitting are: $A_0=0.7$, $\lambda_{\rm sp}=198$ nm, x=50 nm, $L_x=1.74$ μ m, $\varphi=0.7$ π , r=0.3 (red curve), r=0 (blue curve).

electrical field is homogeneous for all interference orders, the peak electric field intensity for the SP interference decays with the grating separation (Figure 4b). This is due to the exponential decay of the SP waves.

Physically, the electrical field between two gratings is the superposition of two SP waves respectively from left and right gratings and their multireflected waves. At point A (50 nm from the center point), the E_z component of the electric field can be described as

$$E_{z}(x) = \sum_{n=0}^{\infty} A_{0} r^{n} e^{n\varphi_{i}} \left\{ e^{-[(2n+1)L/2+x]/L_{x}} e^{2\pi_{i}[(2n+1)L/2+x]/\lambda_{sp}} - e^{-[(2n+1)L/2-x]/L_{x}} e^{2\pi i[(2n+1)L/2-x]/\lambda_{sp}} \right\}$$
(2)

where A_0 denotes the amplitude of the SP wave at the grating edges; L is the cavity length; x is the distance from the cavity center; λ_{sp} and L_x are the SP wavelength and decay length respectively; r is the reflective coefficient of the grating; φ is the phase shift of the surface plasmon waves after the reflection by the grating. Since point A corresponds to a maximum for E_z and negligible minimum for E_x , it is accurate enough to use E_z components to represent total electrical field at this point. The reflection order n in the equation is truncated at 2 since contributions of higher orders are negligible due to the decay of SP waves. The cavity resonance behavior as a function of the grating separation is due to multibeam interferences, and thus disappears if the reflectivity is assumed to be zero (Figure 4b). The fitting of the above model to the simulation data yield a grating reflectivity about 30%. This value is reasonably larger than that of a single groove²² but still not high enough to form an efficient resonance cavity. Therefore, this cavity effect will not affect the lithography patterning much, which is confirmed by quite modest (~10%) variation of the field

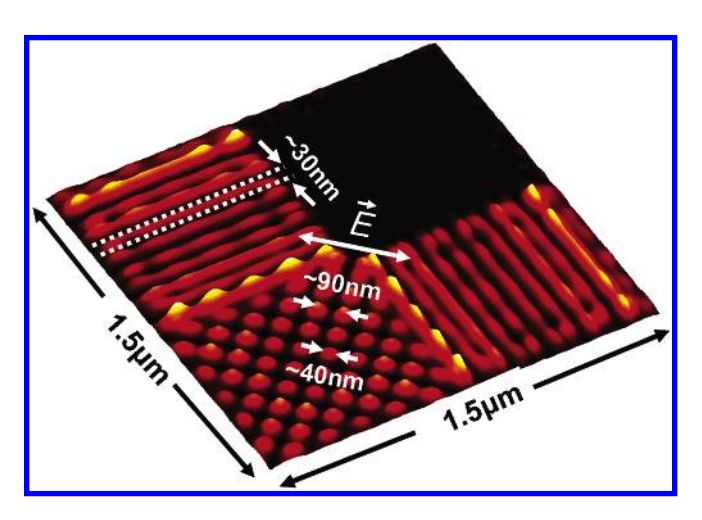


Figure 5. Distribution of the electrical field intensity in the photoresist at z = 20 nm for four perpendicular gratings with 130 nm periodicity. The periodical boundary condition is used for the simulation. The incident light has a 266 nm wavelength and is polarized along the diagonal direction.

and the contrast. Even if this cavity is completely off-resonance (L=2100 nm, for instance), the interference intensity contrast is still as high as 0.4 at the grating edges.

As indicated earlier, the wavelength of the surface plasmon is sensitive to its frequency, therefore the resolution of SPIN can be tuned by varying the excitation frequency. Especially, when the incident light frequency is tuned to be close to the plasmon resonant frequency $\omega_{\rm sp}$, a slight increase in the excitation frequency could lead to significant decrease in the SP wavelengths, which significantly increase the SPIN resolution. However, it comes with the cost of reduction of the plasmon wave decay length that limits the maximum useable area for the interference. In addition to the 1D interference fringes, two-dimensional patterns such as dot arrays can be obtained by crossing more than two surface plasmon waves. For instance, by using a 266 nm exposing light and four mutually perpendicular one-dimensional Al gratings with 130 nm periodicities yield a square lattice of 2D dot array with a 90 nm periodicity and a 40 nm feature size (Figure 5). Although the interference area used in the simulation is $0.75 \,\mu\text{m} \times 0.75 \,\mu\text{m}$, as limited by the computer memory, the pattern region can be considerably enlarged considering that the smallest intensity contrast obtained (about 0.7) is much larger than needed (0.2),

SPIN is different from other surface plasmon assisted lithography techniques, such as nanoparticles printing²³ and tip-enhanced two-photon direct writing by using apertureless metallic AFM tips.²⁴ In those techniques, the whole sample is illuminated, and the exposure of photoresists relies on the local field enhancements by exciting localized surface plasmons. Therefore, the incident light is required to be in certain configuration, especially the polarization needs to be perpendicular to the sample substrates. For SPIN, only a collimated beam is required, and the exposure of samples relies on the interference patterns of propagating surface plasmon waves.

In conclusion, a new nanolithography technique, the surface plasmon interference nanolithography (SPIN), has

been demonstrated by computer simulation. Simulation results have shown that uniform interference patterns far beyond the free-space diffraction limit of the light can be obtained. As examples, one-dimensional grating lines with 100 nm periodicity and two-dimensional dot arrays with 90 nm periodicity have been demonstrated in the simulation using 365 nm and 266 nm exposing light, respectively. This technique provides a new alternative fabrication method for nanodevices.

Acknowledgment. The authors thank J. M. Steele for fruitful discussions. This work was supported by the Center for Scalable and Integrated Nanomanufacturing (SINAM), a NSF Nanoscale Science and Engineering Center (NSEC) under award number DMI-0327077, and a NSF grant (DMI-0218273).

References

- Seidel P.; Canning J.; Mackay S.; Trybula W. Semiconductor FabTech 1998, 7, 147; (http://www.semiconductorfabtech.com/features/lithography/articles/body7.147.php3).
- (2) Schellenberg, F. M. Proc. SPIE, 2004, 5377, 1; Smith, B. W., Ed.
- (3) Mack, C. A. Proc. SPIE 2004, 5374, 1; Mackay, R. S., Ed.
- (4) Chou, S. Y.; Krauss, P. R.; Renstrom, P. J. Science 2001, 272, 85.
- (5) Bailey, T. et al. J. Vac. Sci. Technol. B 2000, 18, 3572.

- (6) Gwyn, C. W.; Stulen, R.; Sweeney, D.; Attwood, D. J. Vac. Sci. Technol. B 1998, 16, 3142. Bates, A. K. et al. IBM J. Res. Dev. 2001, 45, 605.
- (7) Silverman, J. P. J. Vac. Sci. Technol. B 1998, 16, 3137.
- (8) Hoffnagle, J. A.; Hinsberg, W. D.; Sanchez, M.; Houle, F. A. *J. Vac. Sci. Technol. B* **1999**, *17*, 3306.
- (9) Switkes, M.; Rothschild, M. J. Vac. Sci. Technol. B 2001, 19, 2353.
- (10) Ghislain, L. P. et al. Appl. Phys. Lett. 1999, 74, 501.
- (11) Wei, Q. H.; Liu, Z. W.; Luo, Q.; Zhang, X. UCLA invention disclosure **2003**, case number 2003–309, (http://www.research.u-cla.edu/tech/ucla03–309.htm).
- (12) Srituravanich, W.; Fang, N.; Sun, C.; Luo, Q.; Zhang, X. Nano Lett. 2004, 4, 1085.
- (13) Srituravanich, W. et al. J. Vac. Sci. Technol. B 2004, 22, 3475.
- (14) Raether H. Surface Plasmons; Springer-Verlag: Berlin, 1988.
- (15) Luo, X. G.; Ishihara, T. Appl. Phys. Lett. 2004, 84, 4780.
- (16) Luo, X. G.; Ishihara, T. Opt. Express 2004, 12, 3055.
- (17) Johnson, P. B.; Christy, R. W. Phys. Rev. B 1972, 6, 4370.
- (18) Savas, T. A.; Farhoud, M.; Smith, H. I.; Hwang, M.; Ross, C. A. J. Appl. Phys. 1999, 85, 6160.
- (19) Farhoud, M.; et al. J. Vac. Sci. Technol. B 1999, 17, 3182.
- (20) Solak, H. H.; et al. Microelectron. Eng. 2003, 67-68, 56.
- (21) Madou Marc, J. Fundamentals of Microfabrication; CRC Press, Boca Raton, 2002.
- (22) Bouhelier, A. et al. J. Microscopy 1999, 194, 571.
- (23) Kik, P. G.; Martin, A. L.; Maier, S. A.; Atwater, H. A. *Proc. SPIE* **2002**, 4810.
- (24) Yin, X. B.; Fang, N.; Zhang, X.; Martini, I. B.; Schwartz, B. J. Appl. Phys. Lett. 2002, 81, 3663.

NL0506094